Structural effects and 4f-5d transition shifts induced by La-codoping in Ce-doped yttrium aluminum garnet: First-principles study

Ana Belén Muñoz-García,[1] José Luis Pascual,[2] Zoila Barandiarán,[1,3] and Luis Seijo[1,3,*]

[1]*Departamento de Química, Universidad Autónoma de Madrid, 28049 Madrid, Spain*

[2]*Departamento de Química Física Aplicada, Universidad Autónoma de Madrid, 28049 Madrid, Spain*

[3]*Instituto Universitario de Ciencia de Materiales Nicolás Cabrera, Universidad Autónoma de Madrid, 28049 Madrid, Spain*

(Dated: August 3, 2010)

Abstract

According to first-principles calculations performed on Ce-doped and Ce,La-codoped yttrium aluminum garnet (YAG) $Y_3Al_5O_{12}$, the effect of La-codoping on the local structure around Ce defects in Ce:YAG is an anisotropic expansion in overall, in opposition to recent propositions of local lattice compression. Its effect on the lowest Ce^{3+} $4f \rightarrow 5d$ transition is found to be a red shift, in agreement with experiments. The red shift is the result of a decrease of the difference between the energy centroids of the $5d^1$ and $4f^1$ configurations and an increase of the effective ligand field on the Ce-$5d$ shell associated with electronic effects of La substituting for Y. These effects are mitigated by the ligand field decrease associated with the local expansion around Ce, which gives a blue shift contribution of a smaller value. The behavior of the energy difference between the centroids of the configurations cannot be anticipated by the usual model for this quantity, in spite of its usefulness to rationalize $5d \rightarrow 4f$ luminescences. The second $4f \rightarrow 5d$ transition is found to be blue shifted upon La-codoping, also in agreement with experiments.

PACS numbers: 71.55.-i, 61.72.-y, 61.72.J-, 61.72.S-, 71.23.An, 71.70.-d, 78.55.-m

*Corresponding author; Electronic address: luis.seijo@uam.es

I. INTRODUCTION

Yttrium aluminum garnet $Y_3Al_5O_{12}$, or YAG, doped with Ce^{3+} is a blue-to-yellow down-converter phosphor used in white light solid-state lighting devices.[1,2] Controlling the color of these devices is considered one of the important issues governing the success of these technologies[3] and one of the methods used for this purpose is codoping.[4–7] Codopants are long ago known to be able to act as co-activators[6] and as wavelength shifters.[1,8–10] In the case of Ce:YAG, Gd^{3+} and La^{3+} are known to shift the $5d \rightarrow 4f$ yellow luminescence of the Ce^{3+} defects to longer wavelengths (red shift), whereas codoping with Ga^{3+} and In^{3+} shifts the luminescence to shorter wavelengths (blue shift).[1,4,8–10] The effects of these codopants on the $4f \rightarrow 5d$ absorptions have not deserved the same attention as the luminescence. In this respect, the early experiments of Blasse and Bril[1] already showed the same red and blue shifts of the first $4f \rightarrow 5d$ absortion band upon Gd and Ga codoping, respectively. Interestingly, the second $4f \rightarrow 5d$ absortion band was shown to experience the opposite shifts: blue shift upon Gd codoping and red shift upon Ga codoping.

Not much is known on the details of the relationship between the structure of the local defects and the red or blue shift induced by codoping, but an empirical rule states that substitutions of the dodecahedral Y^{3+} by larger ions gives red shift whereas substitutions of the octahedral Al^{3+} by larger ions gives blue shift of the Ce^{3+} $5d \rightarrow 4f$ luminescence (and of the first $4f \rightarrow 5d$ absortion) in Ce:YAG.[4,9,10] However, the lattice constant increases in both types of substitutions[9] and this complicates the interpretations based on the changes in the local crystal field around the Ce^{3+} $5d$ shell created by the codopings.

The red shift of the transition between the lowest $4f^1$ and $5d^1$ levels of Ce:YAG upon Gd and La codoping has been attributed to induced lattice distortions in the neighborhood of Ce.[7,10] The detailed distortions are unknown experimentally. It is known that the larger ionic radii of Gd^{3+} and of La^{3+} with respect to Y^{3+} make the lattice constant increase after this type of doping[7,9] and it has been interpreted that, together with the lattice expansion, the dopings create local compressions around Ce, which increase the ligand field acting on the Ce-$5d$ shell and, consequently, lower the first $5d^1$ level with respect to the $4f^1$ ground state.[7]

In these circumstances, first-principles calculations can help understanding the mechanisms that govern the light wavelength shifts upon codoping, because they can provide the

simultaneous knowledge of the local structures of the substitutional defects at the atomistic level and of the energies of the electronic transitions involved in the luminescence, and, accordingly, of their mutual dependence. This paper is addressed at linking the structural changes induced in Ce:YAG by La-codoping with the energy differences between the local states of the Ce defects of main character Ce^{3+}-$4f^1$ and Ce^{3+}-$5d^1$ that are responsible for the absorptions and luminescences of the Ce:YAG and Ce,La:YAG materials. Since both La and Gd produce the same qualitative shifts in Ce:YAG and they are expected to do it for a common reason,[10] we think the conclusions of this study can be extended to the effects of Gd-codoping. Gd-codoping of Ce:YAG is, however, more complicated to handle than La-codoping from the computational point of view, due to the large number of open-shell electrons in Gd^{3+}.

We report periodic-boundary-conditions density-functional-theory (DFT)[11,12] calculations on the atomistic structures of Ce:YAG ($Y_{2.875}Ce_{0.125}Al_5O_{12}$) and Ce,La:YAG ($Y_{2.75}Ce_{0.125}La_{0.125}Al_5O_{12}$) in their ground states, and wave function based calculations on the ground and excited states of the $(CeO_8)^{13-}$ and $(CeO_8Al_2O_4)^{15-}$ embedded clusters, under the effects of embedding potentials of YAG and La:YAG, using the previous atomistic structures. The latter start with complete-active-space self-consistent-field (CASSCF)[13–15] calculations, which provide optimum (occupied and virtual) orbitals for the embedded clusters in their ground and excited states, and continue with second-order many-body perturbation theory (CASPT2)[16–19] calculations, which provide the ground and excited state energies of the embedded clusters involved in the Ce^{3+} $4f \rightarrow 5d$ optical absorptions.

The calculations show that La-codoping induces a strongly anisotropic distortion around the Ce defects which is an expansion in overall. Also, it induces a red shift of the first Ce^{3+} $4f \rightarrow 5d$ absorption which is in agreement with the experiments. The factors that govern the red shift are clarified by means of the analysis of the evolution of these absorptions with the structural and electronic changes induced by La-codoping. The second $4f \rightarrow 5d$ absorption is found to experience a blue shift.

The details of the calculations are presented in Sec. II, the results are discussed and analyzed in Sec. III and the conclusions presented in Sec. IV.

II. DETAILS OF THE CALCULATIONS

The atomistic structures of the doped materials $Y_{2.875}Ce_{0.125}Al_5O_{12}$ and $Y_{2.75}Ce_{0.125}La_{0.125}Al_5O_{12}$ have been obtained with the periodic boundary conditions self-consistent SIESTA method,[20,21] using density functional theory[11,12] (DFT) within the generalized gradient approximation (GGA) as formulated by Perdew, Burke, and Ernzerhof[22,23] (PBE). We used norm-conserving pseudopotentials[24] in the Kleinman-Bylander form.[25] For Y, Al, and O, we used those previously generated and used in pure YAG;[26] for Ce and La we generated here their relativistic version[27] for the reference configurations $Ce^{3+}(5s^24p^64f^1)$ and $La^{3+}(5s^24p^6)$. Nonlinear partial-core corrections[28] and semicore states to account for large core-valence overlap have been used for Y and La. Atomic basis sets of double-ζ plus polarization quality have been used for all atoms: Y($5s5s'4p4p'5p4d4d'$), Al($3s3s'3p3p'3d$), O($2s2s'2p2p'3d$), Ce($5s6s6s'5p5p'6p5d5d'4f$), and La($5s6s6s'5p5p'6p5d5d'4f$). The basis sets of Y, Al, and O have been generated in Ref. 26 and those of Ce and La have been optimized here in a similar manner, using the fictitious enthalpy method of Anglada *et al.*[29] in $CeAlO_3$ and $LaAlO_3$ perovskites (with lattice constants a =3.82 Å and 3.74 Å respectively). The charge density has been projected on a uniform grid in real space, with an equivalent plane-wave cutoff of 380 Ry, in order to calculate the exchange-correlation and Hartree matrix elements. Total energy calculations have been converged with respect to k-space integration; a k grid cutoff of 15.0 Bohr was used.

All geometry optimizations have been performed without imposing any symmetry restrictions in the positions of all atoms in the unit cell, using a conjugate gradient method, with a force tolerance of 0.04 eV/Å. Starting geometries were generated from the computed atomistic structure of perfect YAG[26] (a=12.114 Å, x(O)=-0.036, y(O)=0.0519 and z(O)=0.1491, in good agreement with experiment,[30]) upon subsitution of Y atoms by Ce and La atoms to generate the single and double substitutional defects. We have explored the change in the volume of the unit cell produced by the substitutional by allowing the cell to breath after optimization of a defect. The small lattice constant increment found in Ce:YAG, +0.11%, made us neglect lattice expansion effects on the defect structures.

The optical absorption energies corresponding to the Ce^{3+} $4f \rightarrow 4f$, $4f \rightarrow 5d$, and $4f \rightarrow 6s$ transitions in Ce:YAG and Ce,La:YAG have been calculated with embedded clus-

ter wave function based methods. For this purpose, the $(CeO_8)^{13-}$ and $(CeO_8Al_2O_4)^{15-}$ clusters were embedded in *ab initio* model potential (AIMP)[31] representations of the pure and La-doped hosts YAG and La:YAG. The first of these clusters is made of the Ce ion and its first eightfold oxygen coordination. The second cluster includes two additional AlO_2 atomic sets chosen in such a manner that the two AlO_4 moieties that share two oxygens each with the CeO_8 unit are included in the cluster (Fig. 1). The AIMP embedding potential of YAG, which includes electrostatic, exchange, and Pauli repulsion interactions between the cluster and its environment, was produced according to the prescriptions in Ref. 32. The embedding AIMP of La^{3+} was taken from Ref. 33. In the $(CeO_8)^{13-}$ and $(CeO_8Al_2O_4)^{15-}$ embedded clusters, spin-orbit free relativistic calculations have been performed using atomistic structures resulting from ground state periodic DFT calculations described above. Bonding, static and dynamic correlation, and scalar relativistic effects are taken into account in state-average complete active space self consistent field (SA-CASSCF)[13–15] plus multistate second-order perturbation theory (MS-CASPT2)[16–19] calculations performed with a scalar relativistic many-electron Hamiltonian. These calculations are performed with the program MOLCAS.[34] Spin-orbit coupling effects are missing in these calculations, but their effect on the $4f \rightarrow 5d$ transitions of Ce:YAG, which are the focus of this paper, are known to be a uniform increment of around 1000 cm^{-1} with negligible dependence on the atomistic structure.[35]

In the SA-CASSCF calculations, a $[4f, 5d, 6s]^1$ CAS was used, meaning that the wave functions are configuration interaction (CI) wave functions of all configurations whith the unpaired electron occupying one of the thirteen molecular orbitals of main character Ce-$4f$, Ce-$5d$, and Ce-$6s$. The molecular orbitals are chosen so as to minimize the average energy of the thirteen states. No symmetry was used in these calculations. Nevertheless, in Ce:YAG, a local D_2 site is found and the states can be classified as follows: the first seven states result from the splitting of the $4f^1\ {}^2F$ atomic term (1^2A, 1^2B_1, 2^2B_1, 1^2B_2, 2^2B_2, 1^2B_3, and 2^2B_3), five states well above result from the splitting of the $5d^1\ {}^2D$ atomic term (2^2A, 3^2A, 3^2B_1, 3^2B_2, and 3^2B_3), and a final state is linked to the $6s^1\ {}^2S$ atomic term (4^2A). In Ce,La:YAG, the point symmetry is lost and the thirteen states belong to the only irreducible representation of the point group C_1. They are classified as $1 - 13^2A$, although the relative energies of the $4f^1$, $5d^1$, and $6s^1$ configurations are mantained, as we will see later, and $1 - 7^2A$ are basically of Ce-$4f^1$ character, $8 - 12^2A$ are basically of Ce-$5d^1$ character, and

13^2A of Ce-$6s^1$ character. Using the CASSCF (configuration interaction) wave functions and the (occupied and virtual) molecular orbitals, MS-CASPT2 calculations are done where the dynamic correlation effects (which are missisng at the CASSCF level) of the $5s, 5p, 4f$ and $5d$ electrons of Cerium and the $2s$ and $2p$ electrons of the eight Oxygen atoms are added.

In these calculations, a relativistic effective core potential ([Kr] core) and a $(14s10p10d8f3g)/[6s5p6d4f1g]$ Gaussian valence basis set from Ref. 36 was used for Ce. For O, a [He] effective core potential and a $(5s6p1d)/[3s4p1d]$ valence basis set from Ref. 37 was used, extended with one p-type diffuse function for anion[38] and one d-type polarisation function.[39] For Al, we used a [Ne] core potential and a $(7s6p1d)/[2s3p1d]$ valence basis set from Ref. 37, which includes one d-type polarisation function.[39] Extra basis set funtions were added in order to improve the degree of orthogonality achieved between the cluster molecular orbitals and the environmental orbitals: the Y^{3+} $3d, 4s, 4p$ and the Al^{3+} $2s, 2p$ atomic orbitals of all Y and Al next to the cluster in Ce:YAG, as obtained in self-consistent embedded-ions calculations on YAG,[35] plus the La^{3+} $4d, 5s, 5p$ atomic orbitals of the La codopant in Ce,La:YAG, as obtained in self-consistent embedded-ions calculations on $LaMnO_3$.[33] These type of calculations, as well as embedding potentials, effective core potentials, and basis sets have previously been used in first-principles simulations of Ce:YAG absorption and luminescence[35] and they are available from the authors.[40]

III. RESULTS AND DISCUSSION

The most relevant interatomic distances in the structures of the single substitutional Ce_Y defect in $Y_{2.875}Ce_{0.125}Al_5O_{12}$ and of the most stable double substitutional Ce_Y-La_Y defect in $Y_{2.75}Ce_{0.125}La_{0.125}Al_5O_{12}$, according to the DFT calculations, are shown in Table I. The binding energy between two single defects to form one double defect is 0.059 eV (5.7 kJ/mol). The stress energy of the double defect is 0.465 eV (44.8 kJ/mol); this is the energy descent when all atoms relax their positions after Ce substitutes one Y and La substitutes another Y. This value is only slightly larger than the sum of the stress energies of the individual defects Ce_Y and La_Y, 0.448 eV (43.3 kJ/mol). The difference (0.017 eV, 1.5 kJ/mol) can be subtracted from the double defect binding energy to give the binding energy between the stressed (unrelaxed) single Ce_Y and La_Y defects to form the stressed double Ce_Y-La_Y defect: 0.042 eV (4.2 kJ/mol). Ce_Y is in a local site with D_2 point symmetry, with four short Ce-O

distances (2.373 Å) and four long Ce-O distances (2.468 Å). Among all the Ce_Y-La_Y double substitutional defects that correspond to one Ce_Y and one La_Y per YAG unit cell, the one where the impurities substitute for the two closest Y atoms results to be the most stable. In other words, according to these calculations, the Ce and La impurities tend to be as close as possible in Ce,La:YAG. The data in Table I reveal that, after the preferred substitutions, Ce and La rearrange themselves and their local environments in such a way that their distance shifts 0.01 Å away from the original Y-Y distance, and the first coordination shell of Ce suffers an overall expansion (of 0.010 Å on average). On average, the four nearest oxygens to Ce in Ce:YAG experience an expansion of 0.019 Å, whereas the other four, more distant oxygens maintain their distance as in Ce:YAG (average expansion of 0.001 Å). One of the latter gets 0.008 Å closer to Ce. The final image is one of La-codoping producing a strongly anisotropic expansion around Ce_Y. This anisotropy makes it very difficult to predict the relative shifts of the individual levels of the Ce^{3+}-$4f^1$ and Ce^{3+}-$5d^1$ configurations with simple arguments.

In Table II, we show the energies of the levels of the Ce-$4f^1$, Ce-$5d^1$, and Ce-$6s^1$ configurations relative to the ground state, as calculated in this work. The shifts experienced by these levels in Ce:YAG upon La-codoping have been calculated as the difference between the results of the $(CeO_8Al_2O_4)^{15-}$ cluster embedded in the AIMP embedding potentials of Ce,La:YAG and Ce:YAG (7th and 5th columns of the Table, respectively), using the atomic coordinates of the two materials that resulted from the previous periodic DFT calculations.

Although we also performed calculations on a smaller $(CeO_8)^{13-}$ embedded cluster, we found very similar results not only for the overall results (the first $4f \rightarrow 5d$ transition was predicted to have a 243 cm^{-1} red shift instead of the 220 cm^{-1} red shift predicted with the larger cluster, and the second a 543 cm^{-1} blue shift instead of 586 cm^{-1}), but also on the analysis of contributions that will be shown below, all of it leading to the same qualitative conclusions. Accordingly, here we only present and discuss the results on the larger cluster $(CeO_8Al_2O_4)^{15-}$.

The results on the smaller $(CeO_8)^{13-}$ cluster can, however, be compared with previous CASPT2 calculations performed on the same embedded cluster,[35] shown in the third column of Table II, in order to see the effects of the different optimized structures (embedded cluster CASPT2[35] and periodic DFT structures) on the $4f^1$ and $5d^1$ levels, because the atomistic structure is the basic difference between the two calculations. As we see in the

third and fourth columns, the results are very similar and their differences are only of a minor importance, which reflects the similarities between both structures and supports the expectation that the conclusions attained in this paper would hold if the structures of the substitutional defects in the doped (Ce:YAG) and the codoped (Ce,La:YAG) materials were obtained in large embedded cluster CASPT2 calculations.

Before we discuss the shift of the $4f \rightarrow 5d$ transitions, we would like to make a remark on the energy of the third $5d^1$ level of Ce:YAG, which is a 3^2A level in the D_2 point symmetry group at a spin-orbit free level of calculation. As we see, all the calculations give this level above 47000 cm^{-1}, no matter the source of atomistic structure and the size of the cluster. Since spin-orbit coupling is expected to increase its energy by around 1000 cm^{-1},[35] we must conclude that the *ab initio* calculations do not support assignments of a level found in some experiments at around 37000 cm^{-1} to the third $5d^1$ level.[7,41] Although early *ab initio* calculations gave a much lower energy for this level (42600 cm^{-1}),[42] which could apparently justify the assignment, they lacked dynamic correlation effects within the $(CeO_8)^{13-}$ cluster, which are very important for spectroscopic calculations, and they used a crude embedding potential for YAG, just made of point-charges, which is now known to be insufficient for these materials.[43] The mentioned assignment has also been revised by Tanner *et al.*,[44] who concluded that the 37000 cm^{-1} band is not due to Ce^{3+} and supported the earlier assignment of Blasse and Bril,[1] also made by Zhao *et al.*,[45] of a level between 44000 and 44800 cm^{-1} as the third $5d^1$ level. Our present calculations reaffirm the previous *ab initio* calculations of Ref. 35 and give a solid support to such an assignment. The overall agreement with experimental $4f \rightarrow 5d$ absorptions remains as reasonable as in Ref. 35, having in mind that the first of them (2^2A) lies at 21700-22000 cm^{-1} and the second (3^2B_3) at 29400 cm^{-1} (Refs. 1 and 45). The fourth and fifth absorptions (3^2B_2 and 3^2B_1 respectively) are hidden by the host absorption. So far, no detailed observations of zero-phonon lines or peak maxima have been done on the $4f^1$ and $6s^1$ levels.

Let us now discuss the shifts of the $4f \rightarrow 5d$ transitions of Ce:YAG upon La-codoping. As we see in Table II, the present calculations predict a red shift (of 220 cm^{-1}) of the first of these absorptions, which is the one that corresponds to the observed emission of the material. This is in agreement with experiments. In effect, red shifts of the $5d \rightarrow 4f$ luminescence of Ce:YAG have been found to appear as a consequence of La-codoping,[8] as well as of Gd-codoping,[1,4,8–10] and red shift of the first $4f \rightarrow 5d$ absorption has also been observed

upon Gd-codoping.[1] The reasons behind the shifts are thought to be mostly structural and the same for Gd and La codopings;[7,8] we will analyze below these reasons in the case of Ce,La:YAG.

Detailed quantitative comparisons between experimental and theoretical values of the red shifts cannot be made because absorption experiments in the specific material studied in this paper, $Y_{2.75}Ce_{0.125}La_{0.125}Al_5O_{12}$, are missing and the shifts are known to be quantitatively different for La and Gd codoping,[8] for absorption and emission,[1] and for different codopant concentrations.[7,9] In any case, we think the computed red shift might be overestimated, because Tien *et al.*[9] obtanied an approximate rate of 80 cm^{-1} red shift per 10 atom % of Gd codoping for the excitation peak of Ce,Gd:YAG, whereas the theoretical 220 cm^{-1} red shift corresponds to 4.1 atom% of La codoping and La produces smaller red shifts than Gd.[8]

Blasse and Bril[1] also measured the effect of Gd-codoping on the *second* $4f \rightarrow 5d$ absorption of Ce:YAG, which resulted to be a blue shift, in opposition to the red shift of the first absorption. They found a 200 cm^{-1} blue shift upon 50 atom % of Gd codoping (from 29400 cm^{-1} to 29600 cm^{-1}). Our result in Table II is also a blue shift for La-codoping. As before, we think the value of 586 cm^{-1} is overestimated. The fact that the shifts of the two first $5d^1$ levels have opposite signs is an indication of the strong anisotropy of the effects of the present codopings, because both states would be expected to shift more or less uniformly under isotropic perturbations, such as uniform increments or decrements of the ligand field. Shifts of higher $5d^1$ states, as well as of $4f^1$ and $6s^1$ states, upon codoping have not been reported, to the best of our knowledge. The calculations predict much smaller shifts of the $4f^1$ states than the lowest $5d^1$ states, and a much larger shift of the $6s^1$ state.

Given that the first-principles calculations provide the right signs of the shifts, not only of the first $4f \rightarrow 5d$ transition (which supports that of the $5d \rightarrow 4f$ luminescence), but also of the second $4f \rightarrow 5d$ transition, it is interesting to analyze the reasons behind the shifts, specially because the interpretation by means of an increase of the ligand field as a consequence of a local compression around Ce (Ref. 7) is not supported by the first-principles structures calculated here and shown above. We must keep in mind that the effective ligand field on the $5d$ shell, as measured by the $5d$ shell splitting, does not only result from the distances between ligands and Ce, but also from bonding and electronic effects in general. Besides, not only the effective ligand field on Ce can change upon La-codoping, but also the energy difference between the averages of the $5d^1$ and $4f^1$ manifolds ($5d^1$ and $4f^1$ centroids),

and both of them can contribute to the red shift of the first transition and the blue shift of the second.

We can use the diagram of Fig. 2 in order to analyze the different contributions of codoping on the individual $4f \rightarrow 5d$ transitons. According to the diagram, the transition energy between the lowest states of the Ce-$4f^1$ and Ce-$5d^1$ electronic configurations, which we will call here $1-4f^1$ and $1-5d^1$ for simplicity, can be expressed as the sum of a centroid contribution and a ligand-field contribution,

$$\Delta E(1-4f^1 \rightarrow 1-5d^1) = \Delta E_{\text{centroid}}(4f^1 \rightarrow 5d^1) + \Delta E_{\text{ligand-field}}(1-4f^1 \rightarrow 1-5d^1)\,. \quad (1)$$

The centroid contribution is the energy difference between the averages of the two configurations,

$$\Delta E_{\text{centroid}}(4f^1 \rightarrow 5d^1) = \frac{1}{5}\sum_{i=1,5} E(i-5d^1) - \frac{1}{7}\sum_{i=1,7} E(i-4f^1)\,, \quad (2)$$

and the ligand-field contribution is the difference between the stabilization energies of the initial and the final states with respect to their configurational averages,

$$\Delta E_{\text{ligand-field}}(1-4f^1 \rightarrow 1-5d^1) = \Delta E_{\text{LF}}(1-4f^1) - \Delta E_{\text{LF}}(1-5d^1)\,, \quad (3)$$

$$\Delta E_{\text{LF}}(1-4f^1) = \frac{1}{7}\sum_{i=1,7} E(i-4f^1) - E(1-4f^1)\,, \quad (4)$$

$$\Delta E_{\text{LF}}(1-5d^1) = \frac{1}{5}\sum_{i=1,5} E(i-5d^1) - E(1-5d^1)\,. \quad (5)$$

$\Delta E_{\text{LF}}(1-4f^1)$ and $\Delta E_{\text{LF}}(1-5d^1)$ are a measure of the effective ligand field strengths on the $4f$ and $5d$ shells, respectively. The same analysis can be applyed to any of the individual $4f \rightarrow 5d$ transitions.

The results of this analysis, as applied to the first and second $4f \rightarrow 5d$ transitions of Ce,La:YAG, is shown in the last column of Table III. In this Table, we also include the energy levels and their analysis in three additional calculations, A, B, and C, which serve to analyze the effects of: (1) the distortion of the first coordination shell of Ce, (2) the distortion of the rest of the lattice, and (3) the electronic effects brought about by La. In calculation A, the CASSCF/CASPT2 calculations on the embedded $(CeO_8Al_2O_4)^{15-}$ cluster correspond to Ce:YAG. In other words, its atomic coordinates are those it has in Ce:YAG

and its embedding potential is that of Ce:YAG. In calculation B, the only change with respect to A is the set of atomic coordinates of the $(CeO_8Al_2O_4)^{15-}$ cluster, which are the ones it has in Ce,La:YAG. The changes from A to B are the direct effects of the first coordination shell distortion. In C, the atomic coordinates of the embedding potentials are those in Ce,La:YAG but we keep using the embedding potential of the Y^{3+} ion instead of the one of La^{3+}, so that the changes from B to C are only due to long-range lattice distortions. Finally, in D we substitute the Y^{3+} embedding potential by the one of La^{3+}, so arriving to the real calculation on Ce,La:YAG. The changes from C to D are solely due to the electronic effects of the La_Y substitutional defect. The analysis of these effects are shown in Table IV.

In the last column of Table IV, we can see that the red shift of the first $4f \rightarrow 5d$ transition (-220 cm^{-1}) has significant ligand field contributions (-97 cm^{-1}) and centroid contributions (-123 cm^{-1}), in similar amounts. The centroid contribution is dominated by the structural distortions (-101 cm^{-1}) and, among them, by the first-shell distortion (-77 cm^{-1}). On the other hand, the ligand field contribution to the red shift is not due to the structural distortions induced by codoping, but to the electronic effects of La itself (-149 cm^{-1}); in fact, the contribution from the structural distortions is a blue shift (+52 cm^{-1}) that results from a reduction of the effective ligand field on the $5d$ shell, which is consistent with the average expansion experienced by the eight oxygens of the first coordination shell of Ce and the rest of the lattice upon La-codoping. This expansion is, in turn, consistent with the fact that the lattice constant of Ce:YAG has been found to increase with Gd and La codoping.[7,9]

The blue shift of the second $4f \rightarrow 5d$ transition (586 cm^{-1}) is mostly due to ligand field effects (709 cm^{-1}), which result mainly from an important rising of the $2-5d^1$ level among the $5d^1$ manifold (of 659 cm^{-1} with respect to the $5d^1$ centroid), most of it due to the first-shell distortion. This result, put together with the small effect that the lattice distortions have on the effective $5d$ ligand field, as we have seen above, indicate large ligand field anisotropies induced by the La-codoping.

It is also remarkable that the $4f-5d$ centroid, $\Delta E_{\text{centroid}}(4f^1 \rightarrow 5d^1)$, is lower upon La-codoping in spite of the fact that the ligands expand around Ce, because the only model which is under use for this quantity, to the best of our knowledge, is that of Judd and Morrison[46–48] and, according to it, the $4f-5d$ centroid should increase when the distances Ce-O increase. In this model, the centroid is exclusively due to the different ligand (oxygen) polarization by a Ce-$4f$ and a Ce-$5d$ electron and the distance between the electron and the

Ce nucleus is assumed to be negligible with respect to the Ce-O distance. This model is useful for a rationalization of $4f-5d$ centroids of lanthanide ions in many hosts[49] but, according to these first-principles calculations, it can be misleading if used for predicting small centroid shifts associated to small ligand distortions around lanthanides. Similar limitations of the model have been found in previous *ab initio* calculations.[50]

IV. CONCLUSIONS

We have performed first-principles DFT calculations on the structure of the single substitutional Ce_Y and double substitutional Ce_Y-La_Y defects in Ce:YAG and Ce,La:YAG, respectively, and CASSCF/CASPT2 wave function embedded cluster calculations on the Ce-$4f^1$ and Ce-$5d^1$ manifolds of the same materials. The calculations show that La-codoping Ce:YAG causes a strongly anisotropic overall expansion of the atomistic structure around the Ce impurities and a red shift of the lowest Ce^{3+} $4f \rightarrow 5d$ transition, together with a blue shift of the second transition of this type. Both shifts are in agreement with experimental observations of La^{3+} and Gd^{3+} induced shifts.[1,7,9] The red shift of the first $4f \rightarrow 5d$ transition has been shown to be the result of a decrease of the difference between the energy centroids of the $5d^1$ and $4f^1$ configurations and an increase of the effective ligand field on the Ce-$5d$ shell associated with electronic effects of La substituting for Y. These effects are mitigated by the ligand field decrease associated with the local expansion around Ce, which gives a blue shift contribution of a smaller value. The change of the energy difference between the centroids of the configurations could not be anticipated by the usual model for this quantity,[46,47] in spite of its usefulness to rationalize $5d \rightarrow 4f$ luminescences.[49]

Acknowledgments

This work was partly supported by a grant from Ministerio de Ciencia e Innovación, Spain (Dirección General de Programas y Transferencia de Conocimiento MAT2008-05379/MAT). A.B.M.-G. acknowledges a contract of the program Personal Investigador en Formación

(Comunidad de Madrid).

---

[1] G. Blasse and A. Bril, J. Chem. Phys. **47**, 5139 (1967).

[2] T. Justel, H. Nikol, and C. Ronda, Angew. Chem. Int. Ed. **37**, 3084 (1998).

[3] J. Brodrick, J. Disp. Technol. **3**, 91 (2007).

[4] Y. Pan, M. Wu, and Q. Su, J. Phys. Chem. Solids **65**, 845 (2004).

[5] Y. S. Lin, R. S. Liu, and B.-M. Cheng, J. Electrochem. Soc. **152**, J41 (2005).

[6] H. S. Jang, W. B. Im, D. C. Lee, D. Y. Jeon, and S. S. Kim, J. Lumin. **126**, 371 (2007).

[7] Y. X. Pan, W. Wang, G. K. Liu, S. Skanthakumar, R. A. Rosenberg, X. Z. Guo, and K. K. Li, J. All. Comp. **488**, 638 (2009).

[8] W. W. Holloway and M. Kestigian, J. Opt. Soc. Amer. **59**, 60 (1969).

[9] T. Y. Tien, E. F. Gibbons, R. G. DeLosh, P. J. Zacmanidis, D. E. Smith, and H. L. Stadler, J. Electrochem. Soc. **120**, 278 (1973).

[10] J. M. Robertson, M. W. van Tol, W. H. Smits, and J. P. H. Heynen, Philips J. Res. **36**, 151 (1981).

[11] P. Hohenberg and W. Kohn, Phys. Rev. B **136**, 864 (1964).

[12] W. Kohn and L. J. Sham, Phys. Rev. **140**, 1133 (1965).

[13] B. O. Roos, P. R. Taylor, and P. E. M. Siegbahn, Chem. Phys. **48**, 157 (1980).

[14] P. E. M. Siegbahn, A. Heiberg, B. O. Roos, and B. Levy, Phys. Scr. **21**, 323 (1980).

[15] P. E. M. Siegbahn, A. Heiberg, J. Almlöf, and B. O. Roos, J. Chem. Phys. **74**, 2384 (1981).

[16] K. Andersson, P.-Å. Malmqvist, B. O. Roos, A. J. Sadlej, and K. Wolinski, J. Phys. Chem. **94**, 5483 (1990).

[17] K. Andersson, P.-Å. Malmqvist and B. O. Roos, J. Chem. Phys. **96**, 1218 (1992).

[18] A. Zaitsevskii and J. P. Malrieu, Chem. Phys. Lett. **233**, 597 (1995).

[19] J. Finley, P.-Å. Malmqvist, B. O. Roos and L. Serrano-Andrés, Chem. Phys. Lett. **288**, 299 (1998).

[20] P. Ordejón, E. Artacho, and J. M. Soler, Phys. Rev. B **53**, R10441 (1996).

[21] J. M. Soler, E. Artacho, J. D. Gale, A. García, J. Junquera, P. Ordejón, and D. Sánchez-Portal, J. Phys.: Condens. Matter **14**, 2745 (2002).

[22] J. Perdew, K. Burke, and M. Ernzerhof, Phys. Rev. Lett. **77**, 3865 (1996).

[23] J. Perdew, K. Burke, and M. Ernzerhof, Phys. Rev. Lett. **78**, 1396 (1997).

[24] N. Troullier and J. L. Martins, Phys. Rev. B **43**, 1993 (1991).

[25] L. Kleinman and D. M. Bylander, Phys. Rev. Lett. **48**, 1425 (1982).

[26] A. B. Muñoz-García, E. Anglada, and L. Seijo, Int. J. Quantum Chem. **109**, 1991 (2009).

[27] G. B. Bachelet, D. R. Hamann, and M. Schlüter, Phys. Rev. B **26**, 4199 (1982).

[28] S. Louie, S. Froyen, and M. Cohen, Phys. Rev. B **26**, 1738 (1982).

[29] E. Anglada, J. M. Soler, J. Junquera, and E. Artacho, Phys. Rev. B **66**, 205101 (2002).

[30] F. Euler and J. A. Bruce, Acta Crystallogr. **19**, 971 (1965).

[31] Z. Barandiarán and L. Seijo, J. Chem. Phys. **89**, 5739 (1988).

[32] J. L. Pascual, N. Barros, Z. Barandiarán, and L. Seijo, J. Phys. Chem. A **113**, 12454 (2009).

[33] A. Sadoc, R. Broer, and C. de Graaf, J. Chem. Phys. **126**, 134709 (2007).

[34] G. Karlström, R. Lindh, P. A. Malmqvist, B. O. Roos, U. Ryde, V. Veryazov, P. O. Widmark, M. Cossi, B. Schimmelpfennig, P. Neogrady, and L. Seijo, Comput. Mater. Sci. **28**, 22 (2003).

[35] J. Gracia, L. Seijo, Z. Barandiarán, D. Curulla, H. Niemansverdriet, and W. van Gennip, J. Lumin. **128**, 1248 (2008).

[36] L. Seijo, Z. Barandiarán, and B. Ordejón, Mol. Phys. **101**, 73 (2003).

[37] S. Huzinaga, L. Seijo, Z. Barandiarán, and M. Klobukowski, J. Chem. Phys. **86**, 2132 (1987).

[38] T. H. Dunning and P. J. Hay, in *Modern Theoretical Chemistry*, edited by H. F. Schaefer III (Plenum, New York, 1977).

[39] J. Andzelm, M. Klobukowski, E. Radzio-Andzelm, Y. Sakai, and H. Tatewaki, *Gaussian Basis Sets for Molecular Calculations*, edited by S. Huzinaga, (Elsevier, Amsterdam, 1984).

[40] Detailed core and embedding AIMP data libraries in electronic format are available from the authors upon request or directly at the address http://www.uam.es/quimica/aimp/Data/-AIMPLibs.html. See also Ref. 34.

[41] T. Tomiki, H. Akamine, M. Gushiken, Y. Kinjoh, M. Miyazato, T. Miyazato, N. Toyokawa, M. Hiraoka, N. Hirata, Y. Ganaha, et al., J. Phys. Soc. Japan **60**, 2437 (1991).

[42] H. Merenga, J. Andriessen, and C. W. E. V. Eijk, Radiat. Meas. **24**, 343 (1995).

[43] J. L. Pascual, J. Schamps, Z. Barandiarán, and L. Seijo, Phys. Rev. B **74**, 104105 (2006).

[44] P. A. Tanner, L. Fu, L. Ning, B.-M. Cheng, and M. G. Brik, J. Phys.: Condens. Matter **19**, 216213 (2007).

[45] G. J. Zhao, X. H. Zeng, J. Xu, S. M. Zhou, and Y. Z. Zhou, Phys. Status Solidi A **199**, 355

(2003).

[46] B. R. Judd, Phys. Rev. Lett. **39**, 242 (1977).

[47] C. A. Morrison, J. Chem. Phys. **72**, 1001 (1980).

[48] M. Bettinelli and R. Moncorgé, J. Lumin. **92**, 287 (2001).

[49] P. Dorenbos, J. Lumin. **87-89**, 970 (2000).

[50] Z. Barandiarán, N. M. Edelstein, B. Ordejón, F. Ruipérez, and L. Seijo, J. Solid State Chem. **178**, 464 (2005).

TABLE I: Selected interatomic distances, in Å, in the Ce_Y subsitutional defect in Ce:YAG and in the most stable Ce_Y-La_Y double substitutional defect in Ce,La:YAG. Oxygen labels correspond to Figure 1. Distance changes around Ce_Y induced by La-codoping are given in parentheses.

Ce:YAG		Ce,La:YAG			
d(Ce-Y)	3.718	d(Ce-La)	3.728 (+0.010)		
			Oxygens of type 1		
d(Ce-O_B)	2.373	d(Ce-O_B)	2.427 (+0.054)	d(La-O_A)	2.417
		d(Ce-O_1)	2.385 (+0.012)	d(La-O_a)	2.412
		d(Ce-O_4)	2.374 (+0.001)	d(La-O_c)	2.399
		d(Ce-O_5)	2.383 (+0.010)	d(La-O_e)	2.416
			Oxygens of type 2		
d(Ce-O_A)	2.468	d(Ce-O_A)	2.470 (+0.002)	d(La-O_B)	2.482
		d(Ce-O_2)	2.460 (-0.008)	d(La-O_b)	2.522
		d(Ce-O_3)	2.513 (0.000)	d(La-O_d)	2.510
		d(Ce-O_6)	2.477 (+0.009)	d(La-O_f)	2.524

TABLE II: Relative energies of the levels of the Ce-$4f^1$, Ce-$5d^1$, and Ce-$6s^1$ configurations of the materials Ce:YAG and Ce,La:YAG and their shift induced by La-codoping Ce:YAG. All numbers in cm^{-1}.

Material:		Ce:YAG			Ce,La:YAG		
Embedded cluster:		$(CeO_8)^{13-}$	$(CeO_8)^{13-}$	$(CeO_8Al_2O_4)^{15-}$		$(CeO_8Al_2O_4)^{15-}$	
	D_2	Ref. 35	This work	This work	C_1	This work	Shift
$4f^1$ levels							
	$1\ ^2B_2$	0	0	0	$1\ ^2A$	0	
	$1\ ^2B_3$	280	274	38	$2\ ^2A$	62	25
	$1\ ^2B_1$	440	290	202	$3\ ^2A$	248	46
	$1\ ^2A$	620	518	416	$4\ ^2A$	490	74
	$2\ ^2B_1$	700	577	443	$5\ ^2A$	541	98
	$2\ ^2B_2$	710	638	516	$6\ ^2A$	620	104
	$2\ ^2B_3$	2710	2530	2419	$7\ ^2A$	2422	4
$5d^1$ levels							
	$2\ ^2A$	23010	24887	23853	$8\ ^2A$	23633	-220
	$3\ ^2B_3$	30670	30187	30169	$9\ ^2A$	30756	586
	$3\ ^2A$	47040	48080	48112	$10\ ^2A$	47659	-454
	$3\ ^2B_2$	51600	49705	48700	$11\ ^2A$	49267	567
	$3\ ^2B_1$	52840	52568	52221	$12\ ^2A$	51376	-845
$6s^1$ level							
	$4\ ^2A$		67133	61214	$13\ ^2A$	63110	1896

TABLE III: $4f^1$, $5d^1$, and $6s^1$ levels of the $(CeO_8Al_2O_4)^{15-}$ cluster in several embedding potentials.

	Calculation			
	A	B	C	D
Cluster coordinates	Ce:YAG	Ce,La:YAG	Ce,La:YAG	Ce,La:YAG
Embedding coordinates	Ce:YAG	Ce:YAG	Ce,La:YAG	Ce,La:YAG
Embedding potential on La_Y	Y	Y	Y	La
	$4f^1$ levels			
$1\ ^2A$	0	0	0	0
$2\ ^2A$	38	43	52	62
$3\ ^2A$	202	218	228	248
$4\ ^2A$	416	455	458	490
$5\ ^2A$	443	498	503	541
$6\ ^2A$	516	562	585	620
$7\ ^2A$	2419	2382	2390	2422
	$5d^1$ levels			
$8\ ^2A$	23853	23861	23803	23633
$9\ ^2A$	30169	30678	30690	30756
$10\ ^2A$	48112	47660	47659	47659
$11\ ^2A$	48700	49157	49123	49267
$12\ ^2A$	52221	51402	51404	51376
	$6s^1$ level			
$13\ ^2A$	61214	62566	62186	63110
$\Delta E_{\text{centroid}}(4f^1 \rightarrow 5d^1)$	40035	39958	39933	39912
$\Delta E_{\text{LF}}(1-4f^1)$	576	594	603	626
$\Delta E_{\text{LF}}(1-5d^1)$	16758	16691	16733	16905
$\Delta E_{\text{ligand-field}}(1-4f^1 \rightarrow 1-5d^1)$	-16182	-16097	-16130	-16279
$\Delta E_{\text{LF}}(2-5d^1)$	10442	9874	9846	9782
$\Delta E_{\text{ligand-field}}(1-4f^1 \rightarrow 2-5d^1)$	-9866	-9280	-9243	-9156

TABLE IV: Analysis of the first and second $4f \rightarrow 5d$ transitions' shift from Ce:YAG to Ce,La:YAG. All numbers in cm^{-1}.

	Contributions			
	First-shell distortion	Full distortion	La	All
$\Delta E_{\text{centroid}}(4f^1 \rightarrow 5d^1)$	-77	-101	-22	-123
$\Delta E_{\text{LF}}(1-4f^1)$	18	26	24	50
	$1-4f^1 \rightarrow 1-5d^1$ transition			
$\Delta E_{\text{LF}}(1-5d^1)$	-68	-25	173	147
$\Delta E_{\text{ligand-field}}$	85	52	-149	-97
ΔE	8	-50	-170	-220
	$1-4f^1 \rightarrow 2-5d^1$ transition			
$\Delta E_{\text{LF}}(2-5d^1)$	-568	-596	-63	-659
$\Delta E_{\text{ligand-field}}$	586	623	87	709
ΔE	509	521	65	586

FIG. 1: Above: Representation of the most stable Ce_Y-La_Y disubstitutiona defect. Below: $(CeO_8Al_2O_4)^{15-}$ (solid line) and $(CeO_8)^{13-}$ (dashed line) embedded clusters used in this work.

FIG. 2: Schematic representation of the $4f^1$ and $5d^1$ manifolds of the Ce_Y substitutional defect in Ce:YAG.

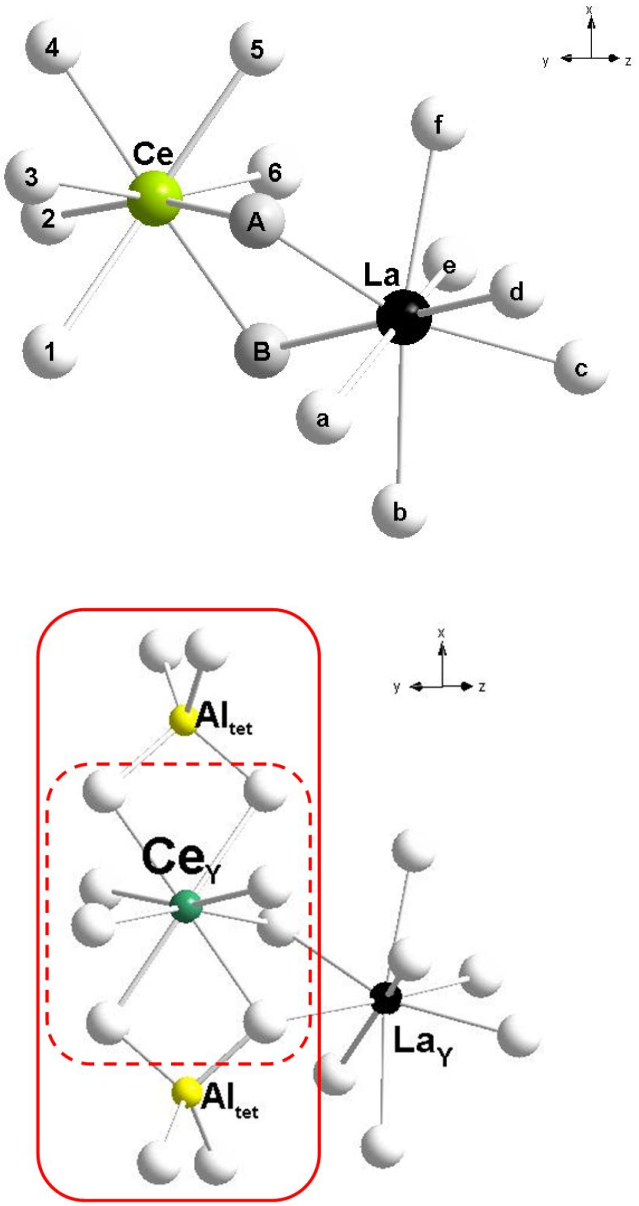

Figure 1 Muñoz-García *et al.*

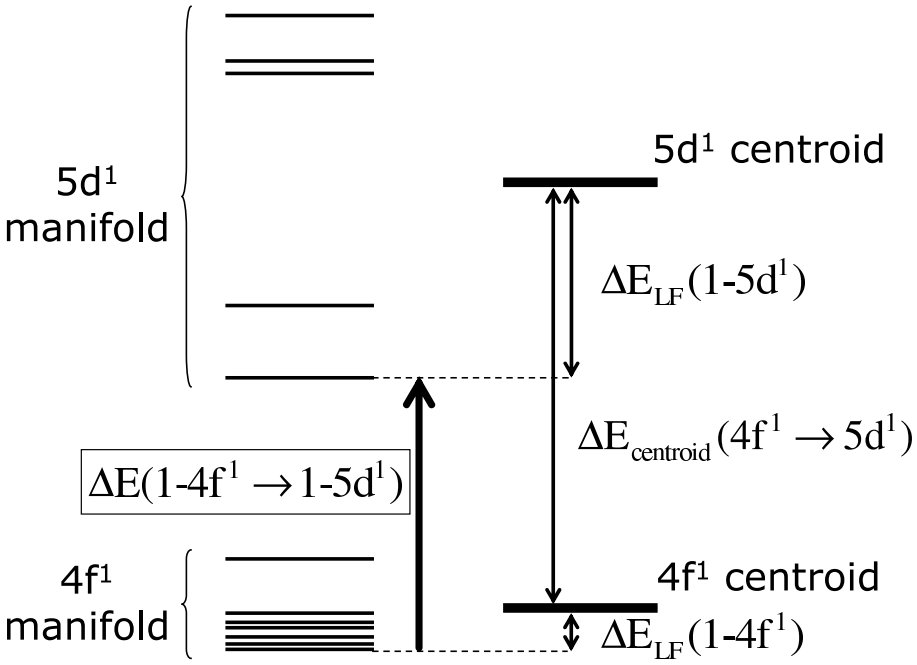

Figure 2 Muñoz-García *et al.*